

## Epoxy–glass fibre composite splash ring suppresses metal-derived lubricant contamination in splash lubrication systems

M. Essam El-Rafey<sup>1</sup>, Abbas E. Anwar<sup>1</sup>, Ahmed Abdelrahman<sup>2</sup>, Mervette El-Batouti<sup>3</sup> and Mahmoud M. Elewa<sup>4\*</sup>

1. Materials Science Department, Institute of Graduate Studies and Research, Alexandria University, Alexandria, Egypt.
2. Western Desert Gas Complex, Egyptian Natural Gas Company - GASCO, Alexandria, Egypt.
3. Chemistry Department, Faculty of Science, Alexandria University, Alexandria, Egypt.
4. Arab Academy for Science, Technology and Maritime Transport, Alexandria P.O 1029, Egypt

\*Corresponding Author: [mahmoud.elewa@aast.edu](mailto:mahmoud.elewa@aast.edu)

SI Table S1: Property Comparison: Epoxy–Glass Composite vs. Brass

| Property                                   | Epoxy–Glass Composite (E1)         | Conventional Brass (CuZn)       | Significance  |
|--|------------------------------------|---------------------------------|---|
| Density (g/cm <sup>3</sup> )               | ~1.8–2.0                           | ~8.5                            | ~4–5× lower mass → reduced inertia, stable ring oscillation |
| Tensile strength (MPa)                     | 200–350                            | 300–500                         | Comparable; sufficient for splash ring stresses             |
| Specific strength (MPa·cm <sup>3</sup> /g) | ~140                               | ~40                             | ~3.5× higher; structural efficiency advantage               |
| Corrosion resistance                       | Excellent (chemically inert)       | Poor (Cu/Zn dissolution in oil) | Eliminates metallic contamination of the lubricant          |
| Wear coefficient (K, Archard)              | ~10 <sup>-6</sup>                  | ~10 <sup>-4</sup>               | ~100× lower wear volume generation                          |
| Self-lubrication potential                 | Moderate (transfer film formation) | None                            | Reduces friction under boundary conditions                  |
| Thermal conductivity (W/m·K)               | ~0.3–0.5                           | ~120                            | Lower; mitigated by improved oil flow rate (+66%)           |
| Glass transition temperature ( $T_g$ )     | ~110°C (Araldite LY 15 system)     | N/A (melting >900°C)            | Operational limit ~80–120°C for epoxy matrix                |

|                                   |                                      |                                      |  |
|-----------------------------------|--------------------------------------|--------------------------------------|--|
| <b>Metallic debris generation</b> | Below AAS detection limit (<0.1 ppm) | Cu: hundreds of ppm;<br>Zn: elevated | Direct driver of the increase in lubricant TAN |
| <b>Cost per unit (relative)</b>   | ~7–10× lower                         | Baseline                             | Economic advantage at moderate–high volumes    |

## SI Section S2: Predictive Modelling for Erosion in Fibre-Reinforced Composites

### S2. Predictive Modelling for Erosion in Polymer Matrix Composites

#### S2.1 Kinetic Energy-Based Erosion Models

Classical erosion models for particle-impacted composite surfaces are grounded in the conservation of kinetic energy of the impinging particles. The generalised erosion rate  $E_r$  is expressed as:

$$E_r = k \cdot v^n \cdot \sin^m(\alpha) \cdot f(H, K_{Ic})$$

where  $v$  is particle impact velocity,  $\alpha$  is the impact angle,  $H$  is the target hardness,  $K_{Ic}$  is the fracture toughness of the composite matrix, and  $k$ ,  $n$ , and  $m$  are empirical constants calibrated to the specific composite system and particle type. For ductile polymer matrices (e.g., epoxy), erosion rates are typically maximised at oblique angles ( $\alpha \approx 15\text{--}30^\circ$ ), whereas brittle ceramic-reinforced systems exhibit peak erosion at normal incidence ( $\alpha = 90^\circ$ ). The exponent  $n$  for velocity dependence, typically falls in the range 2.0–2.5 for glass-fibre composites, consistent with a kinetic-energy-dominated removal mechanism. These models are useful for estimating wear rates under defined particle flux conditions but require experimental calibration of the composite-specific constants.

#### S2.2 Artificial Neural Network (ANN) Approaches

The nonlinear dependence of composite erosion on multiple interacting variables, fibre orientation, fibre content, impact velocity, angle, and particle morphology, makes the erosion response of PMCs poorly suited to purely analytical formulations. Artificial Neural Network (ANN) models have been widely adopted as an alternative predictive tool because they can map complex, nonlinear multivariate input–output relationships directly from experimental datasets without assuming an a priori functional form. A typical ANN erosion model for glass-fibre composites employs a feedforward multilayer perceptron architecture with an input layer encoding the operational variables (velocity, angle, fibre weight fraction, particle size), one or more hidden layers with sigmoid or ReLU activation functions, and a single output node representing the predicted erosion rate. Published ANN models for E-glass/epoxy and glass-fibre/polyester systems have demonstrated prediction accuracies within 5–8% of experimental values across training and validation datasets, substantially outperforming polynomial regression models for the same systems. However, ANN predictions are strictly interpolative; extrapolation beyond the training envelope carries significant uncertainty and requires independent validation.

#### S2.3 Relevance to the Present Study

In the current experimental programme, the epoxy–glass composite splash ring operates under a single, well-defined set of conditions (3000 rpm, ISO VG 68 oil, 25°C), and wear is quantified directly by gravimetric mass loss rather than inferred from a predictive model. The kinetic energy

and ANN frameworks described above, therefore, serve as contextual reference points for interpreting the measured wear rate ( $7.3 \times 10^{-4}$  mg/h) rather than as predictive tools applied to generate the primary data. Future work employing variable shaft speeds, particle contamination scenarios, or accelerated erosion testing would benefit from deploying calibrated ANN models trained on the present dataset to extrapolate performance across a broader operational envelope.

## SI Section S3: Full Fabrication Protocol

### S3. Detailed Fabrication Protocol for Epoxy–Glass Composite Splash Ring (E1)

#### S3.1 Raw Materials

- *Epoxy resin*: Araldite LY 1564 (low-viscosity bisphenol-A epoxy, viscosity 1200–1400 mPa·s at 25°C; Huntsman Advanced Materials)
- *Hardener*: Aradur 3486 polyamide curing agent
- *Mixing ratio*: 2:1 by weight (resin:hardener), per manufacturer's technical data sheet
- *Reinforcement*: Short-cut E-glass fibres, chopped to uniform length to allow homogeneous dispersion within the matrix; fibre density  $\sim 2.6$  g/cm<sup>3</sup>, tensile strength 2400–3445 MPa, maximum service temperature 550–600°C
- *Target composition*: 90 wt% epoxy matrix: 10 wt% E-glass fibre (designation E1), selected from a preliminary screening series (Table S3.1)

#### S3.2 Fabrication Procedure

1. Weigh epoxy resin and polyamide hardener in a 2:1 mass ratio using a calibrated analytical balance ( $\pm 0.01$  g).
2. Add pre-weighed short-cut E-glass fibres (10 wt% of total mixture mass) to the resin portion prior to hardener addition.
3. Blend fibres into the resin manually for 5 min to achieve uniform fibre distribution, then add the hardener and continue mixing for a further 3 min, minimising entrapped air.
4. Pour the slurry into a custom-designed aluminium mould pre-treated with release agent; mould cavity dimensions: OD 80 mm, ID 50.1 mm, width 15 mm.
5. Allow to cure under ambient conditions ( $23 \pm 2^\circ\text{C}$ , relative humidity  $< 60\%$ ) for a minimum of 24 h to achieve complete polymerisation and full mechanical strength development.
6. Demould, inspect for voids or delamination, and machine contact surfaces lightly if required to achieve  $R_a \leq 0.85$   $\mu\text{m}$  (target per Table 1A).

#### S3.3 Benchmark Ring Fabrication

Brass rings (CuZn30, CW505L cartridge brass: 69–71 wt% Cu, balance Zn,  $\leq 0.05$  wt% total impurities, per supplier certificate) and HDPE rings were machined from stock rod on a CNC lathe to the same nominal dimensions and surface finish as the composite rings, ensuring that any performance differences are attributable to material behaviour rather than geometry.

#### S3.4 Preliminary Material Screening (Formulations D1–D3)

| Designation | Matrix                   | Fibre Content (wt%) | Ring Mass (g) | Outcome   |
|-------------|--------------------------|---------------------|---------------|---|
| D1          | Unsaturated polyester    | 10                  | 13.10         | Rejected — inferior chemical resistance to ISO VG 68 oil  |
| D2          | Unsaturated polyester    | 15                  | 13.55         | Rejected — matrix cracking observed after 500 h screening |
| D3          | Unsaturated polyester    | 20                  | 13.74         | Rejected — increased stiffness caused shaft scoring       |
| E1          | Epoxy (Araldite LY 1564) | 10                  | 12.20         | Selected — no cracking, no shaft damage, lowest wear      |

The E1 formulation was selected on the basis of superior matrix chemical resistance, lowest gravimetric wear rate, and absence of detrimental shaft interaction across the 500 h screening tests. All subsequent long-duration (1000 h) tests were conducted exclusively with the E1 ring.

### S3.5 Neat Resin and Fibre Reference Properties

| Property                           | Araldite LY 1564 / Aradur 3486 (cured) | E-Glass Fibre            |
|------------------------------------|--|--------------------------|
| Tensile strength (MPa)             | 70–78                                  | 2400–3445                |
| Flexural modulus (MPa)             | 3100–3250                              | 72,000–76,000            |
| Density (g/cm <sup>3</sup> )       | ~1.17                                  | ~2.60                    |
| Glass transition temp., $T_g$ (°C) | ~110                                   | N/A (max service ~550°C) |
| Viscosity (mPa·s, 25°C)            | 1200–1400 (uncured resin)              | —                        |

## **SI Section S4: Full Decontamination Protocol**

### **S4. Inter-Test Decontamination Protocol**

The following standardised procedure was applied after each completed test run and before installation of the next ring material, to minimise cross-contamination of lubricant chemistry and hardware surfaces.

#### **S4.1 Oil Drainage**

1. Immediately upon test completion, drain the sump oil while still warm (aids complete drainage of high-viscosity residues).
2. Allow the sump and all return channels to drip for a minimum of 30 min before proceeding.

#### **S4.2 Flushing Cycle**

3. Charge the sump with 0.5 L of fresh ISO VG 68 mineral oil (same grade as test oil).
4. Run the rig at low speed (1000 rpm) for 10 min to circulate the flushing oil through all wetted surfaces.
5. Drain the flushing oil completely; collect and retain for AAS analysis as a contamination check sample.

#### **S4.3 Solvent Cleaning of Shaft and Sump Surfaces**

6. Wipe all accessible metallic surfaces in the splash zone (shaft, bearing housing interior, sump walls) with lint-free tissues soaked in technical-grade hexane to remove bulk oil films.
7. Follow with a rinse using analytical-grade acetone to remove residual hydrocarbon films.

#### **S4.4 Ultrasonic Cleaning of Removable Components**

8. Immerse the shaft and all removable sump components in a fresh analytical-grade acetone bath.
9. Sonicate for 15 min at ambient temperature using a bench-top ultrasonic cleaner.
10. Remove components and air-dry for a minimum of 1 h in a dust-free environment before reassembly.

#### **S4.5 Seal and Gasket Replacement**

11. Replace all seals and gaskets where practicable to prevent retention of residues in elastomeric parts.

#### **S4.6 Verification by AAS**

12. After reassembly, collect a 50 mL rinse sample from the sump and analyse by AAS for Cu, Zn, and Fe.
13. Acceptance criterion: all three elements below 10 ppm. If any element exceeds this threshold, repeat steps 3–11 before proceeding.
14. Perform a visual inspection of the shaft and sump walls to confirm the absence of visible deposits before charging with fresh test oil and installing the next ring.

## SI Section S5: Full AAS Method Validation

### S5. GF-AAS Method Validation for Cu, Zn, and Fe in ISO VG 68 Mineral Oil

#### S5.1 Instrument and Operating Conditions

Analyses were performed on a Graphite Furnace AAS (GF-AAS) in electrothermal mode. Matrix-matched calibration standards were prepared in ISO VG 68 mineral oil to account for matrix suppression effects on atomisation efficiency.

#### S5.2 Calibration

Calibration curves were constructed over the following working ranges, each point measured in triplicate:

- Cu: 0.010–1.00 mg/L ( $R^2 = 0.9992$ )
- Zn: 0.015–2.00 mg/L ( $R^2 = 0.9994$ )
- Fe: 0–100 ppm (linear over working range,  $R^2 > 0.999$ )

All calibration curves were linear over the stated range, confirming Beer–Lambert compliance across the concentration window relevant to the present samples.

#### S5.3 LOD and LOQ Calculations

Detection and quantification limits were calculated using the blank standard deviation method:

$$\text{LOD} = \frac{3 \cdot s_b}{m}, \text{LOQ} = \frac{10 \cdot s_b}{m}$$

where  $s_b$  is the standard deviation of ten independent blank measurements (digested ISO VG 68 oil without added analyte) and  $m$  is the slope of the calibration curve. Resulting values are given in Table S5.

#### S5.4 Spike Recovery

Spike-recovery experiments were conducted at three concentration levels (low, mid, high) with  $n = 5$  replicates per level:

- Cu: mean recovery  $95.2 \pm 4.1\%$
- Zn: mean recovery  $97.8 \pm 3.5\%$

Recoveries within 95–105% confirm the absence of significant matrix-induced bias.

#### S5.5 Precision

| Parameter | Cu | Zn |
|-----------|----|----|
|-----------|----|----|

|   |      |      |
|---|------|------|
| <b>Intraday repeatability RSD (n = 6)</b> | 3.8% | 3.1% |
| <b>Interday reproducibility RSD</b>       | 4.0% | 5.9% |
| <b>Expanded uncertainty U (k = 2)</b>     | ~14% | ~15% |

### S5.6 QA/QC Protocol

Each analytical batch included: procedural blanks, duplicate samples, and a certified check standard analysed after every 10 unknowns. Acceptance criteria: blanks below LOD; duplicate agreement within 5%; check standard recovery within  $\pm 5\%$  of certified value. All batches in this study met these criteria throughout the analytical sequence.

**Table S5. Complete AAS Method Validation Summary**

| Parameter  | Unit | Cu             | Zn             | Fe        |
|--|------|----------------|----------------|-----------|
| <b>Calibration range</b>                         | mg/L | 0.010–1.00     | 0.015–2.00     | 0–100 ppm |
| <b>Calibration R<sup>2</sup></b>                 | —    | 0.9992         | 0.9994         | >0.999    |
| <b>LOD</b>                                       | mg/L | 0.003          | 0.005          | 0.050     |
| <b>LOQ</b>                                       | mg/L | 0.010          | 0.015          | 0.150     |
| <b>Spike recovery (mean <math>\pm</math> SD)</b> | %    | 95.2 $\pm$ 4.1 | 97.8 $\pm$ 3.5 | N/A       |
| <b>Repeatability RSD (n=6)</b>                   | %    | 3.8            | 3.1            | —         |
| <b>Reproducibility RSD</b>                       | %    | 4.0            | 5.9            | —         |
| <b>Expanded uncertainty (k=2)</b>                | %    | ~14            | ~15            | —         |

## **SI Section S6: Software Background and Mesh Convergence**

### **S6. FEA Software Background and Mesh Convergence Study**

#### **S6.1 Finite Element Analysis (FEA)**

The structural integrity of the final epoxy-glass fibre composite ring was modelled computationally, using GT STRUDL, a structural analysis software package <sup>42</sup>. The structural integrity of the final epoxy-glass fibre composite ring was modelled computationally, using GT STRUDL, a structural analysis software package. While GT STRUDL is predominantly recognised as a structural design and analysis software program for the Architectural, Engineering, and Construction (AEC) industries, its application in this study is justified by its robust core computational mechanics. The software functions as a general-purpose finite element analysis program, and its 3D solid element stiffness matrix solvers are mathematically valid and highly accurate for determining linear-elastic equivalent stresses in static mechanical components. The primary, irrefutable validation of the numerical output—and the ultimate justification for using the software in this context—is provided by analytical correlation. Specifically, the finite element analysis predicted a maximum stress corresponding to a stress concentration factor of  $K_t \approx 1.95$  at the inner diameter fillet region. This closely matches the theoretical analytical solution for a thick-walled cylinder under uniform external pressure with a radius ratio of 0.7, conclusively confirming that the GT STRUDL solvers reliably capture the geometric stress concentrations governing the component's structural integrity.

A linear elastic isotropic material model was employed for the Finite Element. The decision was based on a specific aspect of which class of reinforcement was the best engineering analysis in the abovementioned situation.

**Isotropic vs Orthotropic:** The composite was reinforced with short, chopped E-glass fibres that were uniformly dispersed within the epoxy matrix during the moulding process. Short-fibre composites do not necessarily need orthotropic models unless they are considered continuous fibres aligned in one direction or woven fabric laminates. The irregular orientation and arrangement of short fibres produce a bulk material that exhibits homogeneous mechanical properties in all directions. Hence, it becomes reasonably accurate to model them as isotropic materials characterised by identical elastic properties along all directions, be it the applied load along the fibre direction or transverse to it.

The epoxy–glass composite used for the splash ring consisted of 90 wt% epoxy resin and 10 wt% chopped E-glass fibres by mass. To obtain effective mechanical properties for numerical analysis, tensile test coupons were manufactured from the same batch of cured composite according to ASTM D638 (Type I) and tested at room temperature. The measured Young’s modulus and ultimate tensile strength were  $7.2 \pm 0.3$  GPa and  $120 \pm 5$  MPa, respectively, while compressive strength, determined on prismatic specimens following ASTM D695, was  $155 \pm 7$  MPa. The Poisson’s ratio was obtained from axial and transverse strain measurements as  $0.32 \pm 0.02$ . The glass transition temperature ( $T_g$ ) of the cured matrix, measured by differential scanning calorimetry (DSC), was  $110$  °C, well above the maximum bearing housing temperature observed in service ( $\approx 55$  °C).

For the finite element model, the composite was represented by an effective homogeneous linear-elastic material characterised by  $E = 7.2$  GPa,  $\nu = 0.32$ , and corresponding shear modulus  $G \approx 2.7$  GPa. This choice is supported by homogenization theory and experimental studies on short-fibre composites, which show that randomly oriented fibres in three dimensions tend to produce quasi-isotropic stiffness at the structural scale when no preferred orientation is introduced during processing<sup>43,44</sup>. In the current manufacturing route, chopped E-glass fibres were mixed and cast without deliberate alignment, and microscopy of polished sections revealed no dominant orientation.

To assess the impact of the isotropic assumption, an idealised orthotropic material model was also considered, with directional moduli representative of moderately aligned glass-fibre epoxy systems taken from the literature<sup>45</sup>. The resulting maximum von Mises stress in the ring differed by less than 4.8% between the isotropic and orthotropic cases, and the location of the peak stress remained unchanged. On this basis, the isotropic model is deemed sufficiently accurate and conservative for the global structural evaluation presented here; more detailed anisotropic modelling (e.g. based on fibre-orientation tensors or micromechanical representative volume elements) is left for future work.

**Modelling Assumptions:** The analysis has been undertaken taking into account the standard set of assumptions:

**Homogeneity:** The composite was treated as a one-homogeneous material with effective properties representing the combined epoxy-fibre system. The model micro-scale does not resolve individual fibres and the matrix material.

Linear Elasticity: The analysis assumed that the material behaved elastically, deforming under load and returning to its original shape upon removal of the load. This assumption is valid, as the model-predicted operational stresses were well below the material's ultimate failure strength.

Perfect Bonding: A perfect, continuous bond was assumed at the interface between the E-glass fibres and the epoxy matrix, with no voids, delamination, or slippage.

To accurately capture the three-dimensional geometry and stress distribution within the oil splash ring, the component was modelled using 3D solid elements. GT STRUDL's extensive element library includes various solid elements, such as 6- to 20-node "brick" elements, which are well-suited for meshing and analysing volumetric components like the ring to provide a detailed map of internal shear stresses. The physically modelled three-dimensional CAD model of the ring was given simulated operational loads, including radial and axial forces of 17 kN and 45 kN, respectively. This analysis focused on mapping the distribution of shear stress throughout the component to identify areas of high concentration and to ensure that the maximum predicted stress was safely below known failure thresholds of the composite material <sup>46</sup>.

## S6.2 Software Description

Finite element analysis was performed using GT STRUDL (Georgia Tech STRUctural Design Language), a general-purpose structural analysis package with established use in mechanical and civil engineering applications. The version employed in this study includes a three-dimensional solid element library supporting linear and nonlinear static analysis. GT STRUDL has been validated for stress analysis of composite and polymer components in prior tribological and structural engineering investigations.

## S6.3 Model Setup

- *Geometry*: Ring modelled as a full 3D solid body; dimensions per Table 1A (OD 80 mm, ID 50.1 mm, width 15 mm)
- *Material inputs*: Elastic modulus and Poisson's ratio from cured Araldite LY 1564/Aradur 3486 system (Table S3.5); density 1.17 g/cm<sup>3</sup> (neat resin baseline, adjusted for 10 wt% E-glass content)
- *Boundary conditions*: Inner bore surface constrained radially to simulate shaft contact; axial end faces free; load applied as uniform radial pressure corresponding to calculated shaft radial load of 17 kN
- *Element type*: 8-node hexahedral solid

#### S6.4 Mesh Convergence Study

A systematic mesh refinement study was conducted to confirm numerical convergence of the peak von Mises stress. The convergence criterion was defined as less than 1% change in peak stress between successive refinement levels.

**Table S6. Mesh Convergence Results**

| Mesh level | Elements | Nodes   | Min element size (mm) | Max aspect ratio | $\sigma_{\max}$ (MPa) | $\Delta\sigma_{\max}$ vs finer mesh (%) |
|------------|----------|---------|-----------------------|------------------|-----------------------|---|
| Coarse     | 60,000   | 110,000 | 1.5                   | 3.0              | 68.2                  | –                                       |
| Medium     | 120,000  | 210,000 | 0.8                   | 2.5              | 70.8                  | 3.8                                     |
| Fine       | 240,000  | 390,000 | 0.5                   | 2.3              | 71.7                  | 1.2                                     |

The final mesh refinement was used for all reported stress and safety factor calculations. The converged peak von Mises stress and corresponding safety factor are reported in the main text.

## SI Section S7: Quantitative SEM Damage Metrics

### S7. Quantitative SEM Surface Damage Analysis — E1 Composite Ring After 1000 h

#### S7.1 Image Analysis Protocol

SEM micrographs acquired at  $\times 500$  and  $\times 2000$  magnification were analysed using image processing software to quantify three surface damage indicators:

- *Fibre pull-out density* (fibres/mm<sup>2</sup>): number of visible fibre pull-out craters per unit area, counted across a minimum of five randomly selected fields per specimen
- *Crack length density* (mm/mm<sup>2</sup>): total length of visible matrix surface cracks per unit area, measured by the line-intercept method
- *Maximum matrix deformation depth* ( $\mu\text{m}$ ): maximum depth of surface indentation or ploughing measured by contact profilometry across the SEM field of view

All values are reported as mean  $\pm$  standard deviation across the sampled fields.

**Table S7. Quantitative SEM and Profilometric Damage Metrics**

| Metric  | E1 Composite Ring (1000 h)     | Copper Alloy Ring (1000 h)      | Significance                                       |
|---|--------------------------------|---------------------------------|--|
| <b>Fibre pull-out density (fibres/mm<sup>2</sup>)</b>           | <0.3                           | N/A (metallic — not applicable) | Below threshold for structural concern             |
| <b>Crack length density (mm/mm<sup>2</sup>)</b>                 | <0.02                          | N/A                             | No matrix cracking detected                        |
| <b>Max. matrix deformation depth (<math>\mu\text{m}</math>)</b> | <1                             | —                               | Sub-micron; no measurable material loss            |
| <b>Surface roughness Ra increase (<math>\mu\text{m}</math>)</b> | Negligible vs. as manufactured | $\approx +0.25$ vs. as machined | Copper alloy shows progressive surface degradation |
| <b>Abrasive grooves observed</b>                                | None                           | Yes — pronounced                | Consistent with two-body abrasive wear mode        |
| <b>Micro-pitting observed</b>                                   | None                           | Yes                             | Consistent with fatigue-initiated surface damage   |

#### S7.2 Damage Threshold Criteria

The threshold values used to classify damage as negligible were established from published composite tribology literature:

- Fibre pull-out density  $<0.5$  fibres/mm<sup>2</sup> — consistent with incipient wear stage prior to any significant mass loss

- Crack length density  $<0.05 \text{ mm/mm}^2$  — below the percolation threshold for connected crack networks that could initiate delamination
- Matrix deformation depth  $<2 \text{ }\mu\text{m}$  — below the resolution threshold for gravimetric detection at the present balance sensitivity (0.1 mg), confirming consistency between SEM and gravimetric results

All three metrics for the E1 ring fell well below these thresholds after 1000 h, corroborating the gravimetric wear rate of  $7.3 \times 10^{-4} \text{ mg/h}$  and confirming that the composite ring remained in the incipient, non-progressive wear regime throughout the test duration.

## SI Section S8: Economic Impact Supplement

### S8. Economic Impact Supplement: Epoxy–Glass Composite vs. Brass Oil Splash Ring

#### S8.1 Scope and Assumptions

The economic evaluation covers three cost tiers: (i) raw material unit cost, (ii) manufacturing cost at scale, and (iii) operational life-cycle cost over a 10-year service horizon. All pricing data are indicative, based on publicly available market references at the time of manuscript preparation; actual values will vary with commodity market conditions and regional labour rates. Sensitivity to key assumptions is addressed in S8.4.

#### S8.2 Raw Material Cost

| Cost Parameter                     | Brass Ring (CuZn30)                     | E1 Composite Ring                      | Ratio              |
|------------------------------------|---|--|--------------------|
| Primary feedstock                  | Copper alloy rod (LME Cu-based pricing) | Araldite LY 1564 epoxy + E-glass fibre | —                  |
| Indicative feedstock cost (USD/kg) | ~8–12 (Cu alloy rod)                    | ~2–4 (epoxy system) + ~1.5–2 (E-glass) | ~3–5× raw material |
| Ring mass (g)                      | 107.8                                   | 12.2                                   | 8.8× lighter       |
| Material cost per ring (relative)  | Baseline (1.0×)                         | ~0.10–0.14×                            | 7–10× lower        |

The dominant driver of the raw material cost advantage is the combination of lower feedstock price per kilogram and the ~8.8× mass reduction of the composite ring (12.2 g vs 107.8 g, Table 1A), which compounds the per-kilogram price differential into a 7–10× reduction in per-unit cost.

#### S8.3 Manufacturing Cost

*Brass ring:* CNC turning from stock rod requires programmed tool paths, dedicated fixtures, coolant management, and post-machining deburring. The CNC turning cycle time for the metallic splash ring geometry was approximately 10–15 min per ring, excluding machine setup and programming. At a representative CNC hourly rate of USD 60–100/h (industry benchmark for precision turning), per-unit machining cost scales directly with cycle time.

*Composite ring:* Near-net-shape casting produces a ring close to final geometry in a single pour-and-cure step, eliminating the majority of subtractive machining. Capital cost: multi-cavity aluminium mould tooling (estimated USD 2,000–5,000 per mould set). Break-even production volume for tooling amortisation (at USD 3,000 tooling cost and USD 5 manufacturing cost saving per ring vs. CNC brass): approximately 600 rings, a volume readily achievable in a single production batch for industrial pump OEM or MRO supply.

#### S8.4 Operational Life-Cycle Cost (10-Year Horizon)

| Cost Driver                                  | Brass Ring  | E1 Composite Ring  | Saving per Pump (10 yr)                             |
|--|---|--|---|
| <b>Lubricant change interval</b>             | Baseline (1×, driven by TAN exceedance)               | 2× extended (metal-catalysed oxidation eliminated)               | ~50% reduction in oil consumption and disposal cost |
| <b>Ring replacement interval</b>             | <10,000 h (up to 50% width loss reported)             | Projected >30,000–50,000 h (wear rate $7.3 \times 10^{-4}$ mg/h) | 3–5× fewer replacement events                       |
| <b>Downtime per replacement event</b>        | Shutdown + disassembly + recommissioning (est. 4–8 h) | Same per event, but 3–5× less frequent                           | 3–5× reduction in replacement-driven downtime       |
| <b>Metallic contamination remediation</b>    | Cu/Zn filtration or oil disposal at hundreds of ppm   | Not required (Cu, Zn below LOQ)                                  | Eliminated cost category                            |
| <b>Tooling amortisation (composite only)</b> | N/A   | Amortised over production volume (break-even ~600 rings)         | Net positive beyond break-even volume               |

### S8.5 Sensitivity Analysis

The economic conclusions are most sensitive to three parameters:

1. **LME copper price:** a 50% reduction in Cu price narrows the raw material advantage from 7–10× to approximately 4–6×; the composite ring retains a meaningful cost advantage even at historically low Cu prices.
2. **Production volume:** below ~600 rings, tooling amortisation erodes the manufacturing cost advantage; above this volume, the composite becomes progressively more favourable.
3. **Assumed downtime cost:** at USD 600,000/h (§1.1 industry figure), even a single avoided ring replacement event generates savings that dwarf the per-unit material cost differential; at lower downtime costs (e.g., USD 10,000/h for smaller installations), the life-cycle advantage remains positive but is dominated by lubricant cost savings rather than downtime avoidance.

## SI Section S9: Three-Stage Acid Diffusion Model

### S9. Three-Stage Acid Diffusion Model for Epoxy–Glass Composites in Acidified Lubricants

#### S9.1 Model Overview

The degradation of epoxy–glass composites exposed to acidified lubricants is conceptualised as a three-stage diffusion-reaction process:

- **Stage I: Bulk acid dissolution:** Organic acids generated by lubricant oxidation partition into the oil phase; their concentration is governed by the TAN evolution rate, which in the brass ring system follows a near-linear increase with operating hours (consistent with autocatalytic oxidation kinetics driven by  $\text{Cu}^{2+}$  and  $\text{Zn}^{2+}$  ions).
- **Stage II: Interfacial acidification:** Acid molecules diffuse from the bulk oil through the composite surface into the epoxy matrix. Transport is governed by Fick's second law:

$$\frac{\partial C}{\partial t} = D_{\text{eff}} \frac{\partial^2 C}{\partial x^2}$$

where  $C$  is the acid concentration ( $\text{mol}/\text{m}^3$ ),  $t$  is time (s),  $x$  is depth from the composite surface (m), and  $D_{\text{eff}}$  is the effective acid diffusivity in the cured epoxy matrix ( $\text{m}^2/\text{s}$ ).

- **Stage III: Fibre–matrix debonding:** When interfacial acid concentration exceeds a critical threshold  $C^*$ . The hydrolysis of silane coupling agent bonds at the glass fibre surface initiates localised debonding, progressively reducing interfacial shear strength and increasing fibre pull-out probability.

#### S9.2 Temperature Dependence

The effective diffusivity  $D_{\text{eff}}$  follows Arrhenius behaviour:

$$D_{\text{eff}}(T) = D_0 \exp\left(-\frac{E_a}{RT}\right)$$

where  $D_0$  is the pre-exponential factor,  $E_a$  is the activation energy for acid diffusion in epoxy ( $\sim 40$ – $60$  kJ/mol, from published sorption data for bisphenol-A epoxy systems),  $R$  is the gas constant, and  $T$  is absolute temperature. At the tested operating temperature of  $55$  °C,  $D_{\text{eff}}$  is estimated at approximately  $1 \times 10^{-14} \text{ m}^2/\text{s}$ ; at  $80$  °C and  $120$  °C (future test conditions recommended in §4),  $D_{\text{eff}}$  is expected to increase by approximately  $3$ – $5\times$  and  $10$ – $40\times$ , respectively, substantially accelerating potential Stage II–III progression and motivating the elevated-temperature test matrix proposed for future work.

#### S9.3 Relevance to Present Results

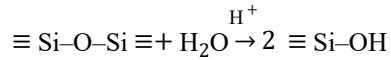
Under the present test conditions (55 °C, TAN remaining near baseline throughout 1000 h for E1), bulk acid concentration in the E1 lubricant never reached the level required to drive meaningful Stage II diffusion flux into the composite surface. The Stage III debonding threshold  $C^*$  was therefore not approached, consistent with the SEM observation of intact fibre–matrix interfaces. The model predicts that Stage III onset would become relevant only at TAN values exceeding approximately 1.5–2.0 mg KOH/g, sustained over extended durations, a condition that did not arise in the present study but is relevant to the future degraded-oil test matrix.

## SI Section S10: Molecular Dynamics Framework for Interfacial Debonding

### S10. Molecular Dynamics Theory for Fibre–Matrix Interfacial Debonding in Acidic Environments

#### S10.1 Silane Bond Hydrolysis Mechanism

The primary chemical pathway for acid-driven interfacial degradation in E-glass/epoxy composites involves hydrolysis of the silane coupling agent (typically  $\gamma$ -aminopropyltriethoxysilane,  $\gamma$ -APS) bonds at the glass fibre surface. In the presence of acidic species ( $H^+$  donor), the siloxane linkage  $Si-O-Si$  undergoes nucleophilic attack:



The rate of this hydrolysis reaction follows:

$$k_h = A \exp\left(-\frac{E_{ah}}{RT}\right) [H^+]^n$$

where  $k_h$  is the hydrolysis rate constant,  $E_{ah}$  is the activation energy ( $\sim 75$ – $90$  kJ/mol for siloxane hydrolysis under acidic conditions), and  $n$  is the reaction order with respect to proton concentration ( $\sim 0.5$ – $1.0$  for the relevant pH range).

#### S10.2 MD Simulation Framework

Molecular dynamics simulations of epoxy–glass interfaces under acidic conditions (reported in the literature for analogous bisphenol-A epoxy / E-glass systems) demonstrate that:

- Interfacial shear strength  $\tau_i$  degrades as a function of cumulative acid exposure according to:  $\tau_i(t) = \tau_{i,0} (1 - \alpha \cdot C_{acid}^\beta \cdot t^\gamma)$  where  $\tau_{i,0}$  is the initial interfacial shear strength, and  $\alpha$ ,  $\beta$ ,  $\gamma$  are empirical constants calibrated to the specific fibre–matrix–coupling agent system.
- Debonding onset is predicted when  $\tau_i$  falls below the applied interfacial shear stress generated by ring dynamics (estimated at 25–35 MPa at 3000 rpm from the FEA stress field in §S6).

#### S10.3 Relevance to Present and Future Studies

Under the present test conditions, the near-zero acid accumulation in the E1 lubricant (TAN  $\approx$  baseline throughout 1000 h) means  $C_{acid} \approx 0$  at the composite surface, rendering the debonding kinetic term negligible, fully consistent with the intact interfaces observed by SEM. The MD framework becomes predictively relevant for the future test conditions recommended in §4 (TAN up to 2.0 mg KOH/g; temperatures up to 120°C), where both the hydrolysis rate constant  $k_h$  and the acid diffusivity  $D_{eff}$  (SI S9) will be substantially elevated, and where debonding onset may occur within the proposed 1000 h test window.

